Computers and Concrete, *Vol. 25, No. 6 (2020) 517-523*
DOI: https://doi.org/10.12989/cac.2020.25.6.517

Dynamic fracture catastrophe model of concrete beam under static load

Zhonggou Chen[1], Chuanqing Fu[2], Yifeng Ling*[3] and Xianyu Jin[4]

[1]*School of Landscape Architecture, Zhejiang Agriculture and Forestry University, Hangzhou 311300, China*
[2]*College of Civil Engineering and Architecture, Zhejiang University of Technology, Hangzhou 310034, China*
[3]*National Concrete Pavement Technology Center, Institute for Transportation, IA 50014, USA*
[4]*College of Civil Engineering and Architecture, Zhejiang University, Hangzhou 310058, China*

(*Received November 12, 2019, Revised April 25, 2020, Accepted May 18, 2020*)

Abstract. An experimental system on three point bending notched beams was established to study the fracture process of concrete. In this system, the acoustic emission (AE) was used to build the cumulative generation order (AGO) and dynamically track the process of microcrack evolution in concrete. A grey-cusp catastrophe model was built based on AE parameters. The results show that the concrete beams have significant catastrophe characteristic. The developed grey-cusp catastrophe model, based on AGO, can well describe the catastrophe characteristic of concrete fracture process. This study also provides a theoretical and technical support for the application of AE in concrete fracture prediction.

Keywords: concrete; damage; catastrophe model; grey-cusp theory; acoustic emission

1. Introduction

The internal fracture of concrete can destroy concrete structures because the propagation of cracks is very rapid and unpredictable (Fan *et al*. 2016). Therefore, the investigations of dynamic fracture process in concrete has been widely conducted among concrete researchers (Choi and Cheung 1994, Choi and Cheung 1994).

Nowadays, acoustic emission (AE) technology has been widely used to detect internal damage of reinforced concrete structures and materials (Behnia *et al*. 2014) to achieve real-time monitoring of damage behavior of structures or components under different loading conditions such as bending, freeze-thaw cycles, fatigue and chemical corrosion. It is used to determine the time of damage occurrence based on the activity, intensity, location and nature of AE source (Xu *et al*. 2013, Mainali *et al*. 2015, Wiedmann *et al*. 2017, Ohno and Ohtsu 2010). The analysis and evaluation of internal damage of concrete can be achieved by processing AE parameters (Nair and Cai 2010, Barrios and Ziehl 2012, Pisani 2018, Sagar and Prasad 2012). Zhou *et al*. evaluated the correlation between AE signals and concrete strength (Zhou *et al*. 2016). The commonly used processing analysis techniques include modal analysis, spectrum analysis, wavelet analysis, artificial neural network pattern recognition and gray correlation analysis (Asamene *et al*. 2015, Pazdera *et al*. 2016, Mostafapour *et al*. 2014, Wang *et al*. 2014, Jiang *et al*. 2016, Li 2013). Huo *et al*. located internal damage in reinforced concrete beams using piezoelectric transducers and AE sensors (Huo *et al*. 2017). However, due to the presence of noise, they usually need a higher threshold which lags acquisition of results behind structural damage and makes structure monitoring difficult (Desa *et al*. 2018, Abouhussien and Hassan 2015, Di Benedetti *et al*. 2013).

In this paper, a three-point bending test was conducted on the notched concrete beams. During the test, AE was used to dynamically track the whole process of microcrack development. Based on the obtained AE signal parameters, a concrete catastrophe model was established using grey-cusp theory. The model was used to predict concrete fracture process and provide a theory for the application of AE technology in the prediction of concrete fracture instability.

2. Grey-cusp catastrophe model

Catastrophe model was firstly proposed by Rene Tom in 1972. After several improvements from scholars, it was separated to many models to study catastrophe that may occur in smooth systems (Zhai *et al*. 2019). Among them, the cusp catastrophe model has been popularly used because it is simple in form, and can better describe the process of catastrophe in the force of external continuous action (Li 2013). The Grey-cusp Theory proposed by Deng Julong (1982) is an effective way to speculate the whole system behavior from finite information, and establish mathematical models for random, incomplete and discrete data (Yuan *et al*. 2010, Chu and Jiang 2009, Li *et al*. 2017, Li *et al*. 2007).

AE is a phenomenon of localized stress concentration in a material, which rapidly releases energy and generates transient elastic waves, also called stress wave emission (Abdelrahman *et al*. 2019). The source associated with the microscopic fracture process of non-metallic material is named AE source (Xie *et al*. 2018, Rodríguez and Celestino 2019, Zohari *et al*. 2013). Under the action of stress, cracks

*Corresponding author, Ph.D.
E-mail: yling@iastate.edu

http://www.techno-press.org/?journal=cac&subpage=8
ISSN: 1598-8198 (Print), 1598-818X (Online)

inside concrete continuously develop, propagate, and will have different AE signal parameters in different fracture stages (Yuyama *et al*. 2001, Carpinteri *et al*. 2008, Iturrioz *et al*. 2013). If the variable causing AE change is uniformly represented by x, the AE sequence during concrete fracture process can be described as a univariate function $f(x)$. Based on the theory of cusp catastrophe (Zhai *et al*. 2019), the potential function of the model is expressed as

$$\mathrm{f(x)}=\left(\frac{1}{4}\right)x^4+\left(\frac{1}{2}\right)ux^2+vx \tag{1}$$

Where y is the AE parameter; x is the mechanical parameter; u and v are the parameters of the relationship between the AE parameter and the mechanical parameter. Eq. (1) can obtain the equilibrium surface equation of the model through derivation once

$$x^3+ux+v=0 \tag{2}$$

Its bifurcation set equation is

$$\Delta=4u^3+27v^2 \tag{3}$$

In Eq. (3), Δ is the value of the bifurcation set equation.

Eq. (3) is a half cube parabola, and the control variable plane is divided into two regions of $\Delta>0$ and $\Delta\leq0$. When $\Delta>0$, the change of v only causes a continuous change of x, and the system is stable at this time; when $\Delta\leq0$, the change of v will cause a jump of x, and the system is in an unstable state.

Grey-cusp theory is a new method to study the problem lack of data and information certainty. It extracts valuable information through the generation and development of gray system information. By learning the uncertainty of small samples and information, the accurate description of the evolution of events and the effective monitoring of behavior are achieved. In the process of dynamic monitoring of AE signals, the actual collected AE parameter sequence tend to be less regular and have a certain oscillation. In order to improve the utilization efficiency of information in parameters and reduce the randomness of parameters in acquisition process, transmission process and statistical process, this paper used gray-cusp theory to accumulate data of AE in the experiment, and then establish the grey-cusp catastrophe model of the system.

Let $x^{(0)}$ be the parameter sequence of a certain AE process, and $x^{(1)}$ is its cumulative generation order (AGO), which are

$$x^{(0)}=\left\{x^{(0)}(1),x^{(0)}(2),\cdots,x^{(0)}(m)\right\} \tag{4}$$

$$x^{(1)}=\left\{x^{(1)}(1),x^{(1)}(2),\cdots,x^{(1)}(m)\right\} \tag{5}$$

Where $x^{(0)}(k)(k\leq m)$ is the gray parameter sequence of k time, and $x^{(1)}(k)$ is its AGO, i.e.

$$x^{(1)}(k)=\sum_{j=1}^{k}x^{(0)}(j)(k\leq m) \tag{6}$$

If the generated sequence $x^{(1)}$ is expanded into a power series at a certain AE process time (t), then Eq. (6) can be written as

$$x^{(1)}(t)=A_0+A_1t+A_2t^2+A_3t^3+\cdots+A_nt^n \tag{7}$$

Where, A_0, A_1, …, A_n, … are undetermined coefficients, which can be obtained by polynomial fitting. Eq. (7) is the fitting polynomial of AGO. According to the literature, the first 5 items (Pazdera *et al*. 2016) are intercepted, which is a new sequence expression

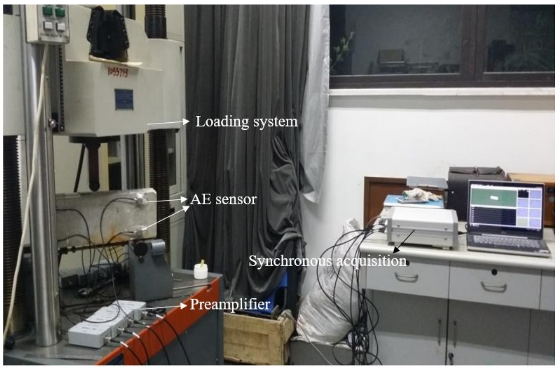

Fig. 1 Three-point bending test setup

$$\hat{x}^{(1)}(t)=A_0+A_1t+A_2t^2+A_3t^3+A_4t^4+A_5t^5 \tag{8}$$

deriving (8) to be

$$y=\frac{d\hat{x}^{(1)}(t)}{dt}=A_1+2A_2t+3A_3t^2+4A_4t^3+5A_5t^4 \tag{9}$$

By substituting variables for the AE parameter sequence in Eq. (9), the standard form of the grey-cusp catastrophe model can be obtained as

$$y=f(t)=(1/4)t^4+(1/2)ut^2+vt+c \tag{10}$$

Where

$$u=\frac{30A_5q^2-12A_4q+3A_3}{\sqrt{5A_5}}(A_5>0) \tag{11}$$

$$u=\frac{30A_5q^2-12A_4q+3A_3}{\sqrt{-5A_5}}(A_5<0) \tag{12}$$

$$q=A_4/5A_5 \tag{13}$$

$$v=\frac{-20A_5q^3+12A_4q^2-6A_3q+2A_2}{(20A_5)^{1/4}}(A_5>0) \tag{14}$$

$$v=\frac{-20A_5q^3+12A_4q^2-6A_3q+2A_2}{(-20A_5)^{1/4}}(A_5<0) \tag{15}$$

Since c is meaningless for catastrophe analysis, it is usually discarded when applied (Wang *et al*. 2014).

3. Test methods

The three-point bending test for the notched concrete beam is shown in Fig. 1 (Fu *et al*. 2015, Fu *et al*. 2019). The test consists of a loading system and an AE system. The loading system used was the Shanghai Hualong Hydraulic Universal Testing Machine, which recorded the force-time curve in real time. The AE system with eight-channel DS2-B series produced by Beijing Ruandao Technology was applied to dynamically track the process of concrete

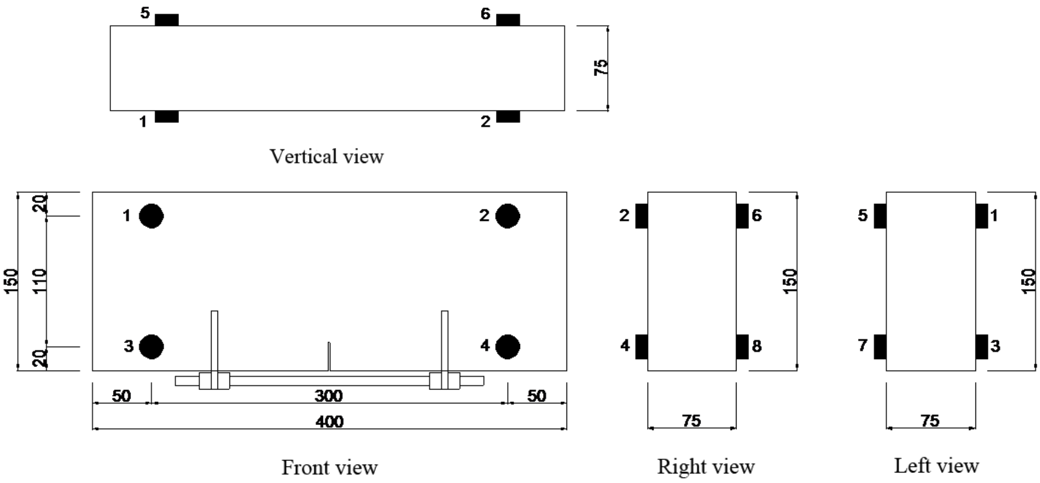

Fig. 2 Locations of RS-2A AE sensors (mm)

Table 1 Mineral ingredient of Portland cement

Composition	C_3S	C_2S	C_3A	C_4AF	Gypsum content
Content (%)	55.5	19.1	6.5	10.1	5.0

Table 2 Mixing proportion (kg/m^3) and strength of concrete (MPa)

w/b	Cement	Fine aggregate	Coarse aggregate	Water	Cube compressive strength
0.53	370	750	1112	188	50.6

fracture. The system collected all AE signals from concrete beam fracture during the test, and recorded the waveform, parameters, numerical values, locations of each point in a laptop. The test was performed with a channel threshold of 40dB. The AE sensor of RS-2A type had frequency range of 50kHz-400kHz, connecting with a preamplifier of 40dB and a multi-channel synchronous acquisition. The acoustic coupling agent on the surface of sensor and specimen was high vacuum grease.

3.1 Test conditions

A Type I Portland cement was used. Coarse aggregate was gravel in 5-20 mm continuous grading. Fine aggregate (river sand) has fineness modulus of 2.64 and water content of 1.2%. Tap water was used as mixing water. The concrete 28-day compressive strength was 50.6 MPa. The concrete beams in dimension of 75 mm×150 mm×400 mm were cast and cured under 20°C and 90% relative humidity for 28 days before test. The depth of notch was 15 mm at the middle of span.

3.2 Test plan

As shown in Fig. 2, using the control screws on test specimen, the specimen did not exhibit brittle fracture, and the crack width was accurately controlled. The sensors of AE system were set by four RS-2A independent-channel sensors mounting on both lateral sides of specimen. Their locations are presented in Fig. 2. All AE signals in the positioning range during the test were captured in an all-round way, and AE waveforms and parameters were completely collected. AE dynamic monitoring on three specimens was carried out in the test.

4. Results and discussion

4.1 Process of AE signal

Fig. 3 shows the process of AE signal changing over time under three-point bending test. Fig. 3(a) presents the variation of ringing count over time. It can be seen that the AE ringing count had two peaks. The first peak appeared at the initial stage of loading, while the second one came after cracking and lasted until the unstable failure. The results of AE hits and AE energy are shown in Fig. 3(b) and Fig. 3(c) respectively, which illustrate that they displayed consistently with the ringing count. A large amount of energy was released at the moments of cracking and final unstable failure of specimen. Fig. 3(d) shows the cumulative counts of AE signal, which indicates that the cumulative counts suddenly increased after cracking.

According to the relationship between the macroscopic deformation response and the microscopic evolution of fracture, the AE signal parameters of the specimen, as shown in Fig. 3, can be divided into four stages: (1) Initial compaction stage, where the AE signal generated immediately after loading, the ringing count raised sharply and the concrete began to crack. (2) Stable growth stage of microcrack, where the cumulative counts continued to climb slowly, but the rates of counting and energy releasing were small. It implies that after the original microcrack, new cracks were continuously produced and the concrete fracture was accumulating. (3) Initial crack stage, where AE hit count and released energy increased rapidly, and concrete internal fracture began to deteriorate. With microcracks spreading, they accumulated and evolved into micro-fracture zones. As a result, cracks occurred in concrete. (4) Fracture failure stage, where the concentration of microcracks was getting stronger, due to the interaction between the channel element and the blocking element. The accumulated energy was released in the form of elastic

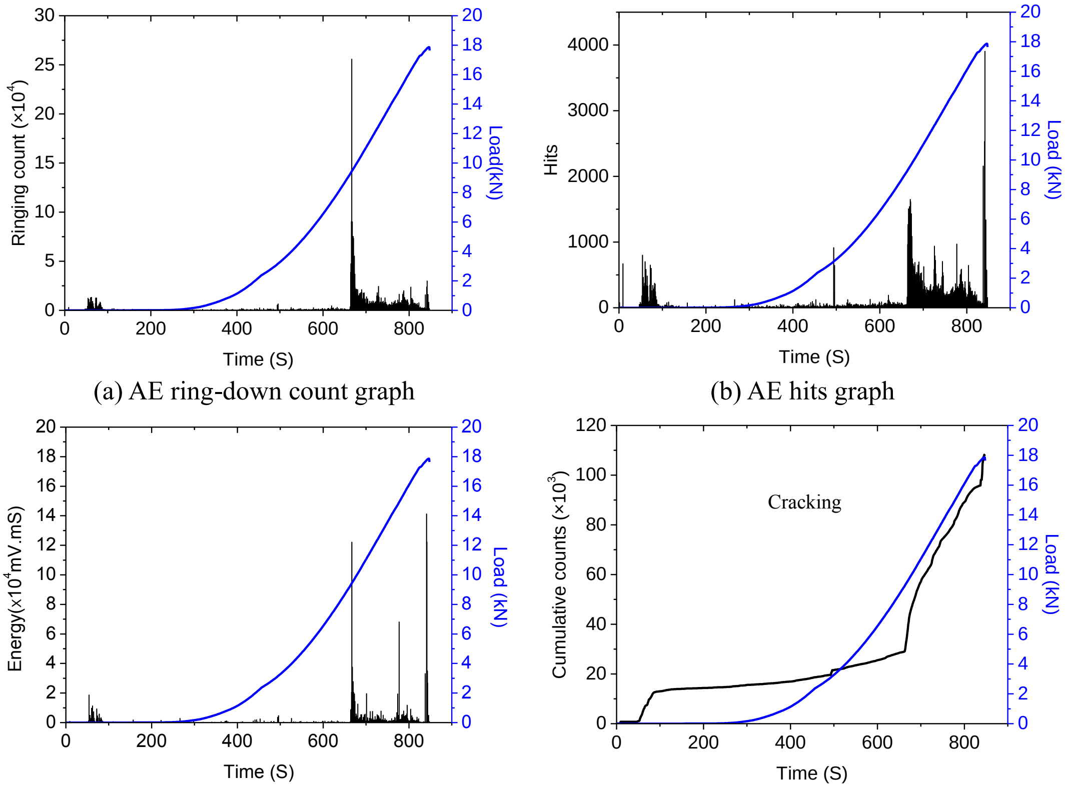

(a) AE ring-down count graph (b) AE hits graph

(c) AE energy graph (d) Cumulative curve of AE hits

Fig. 3 The process of AE signal changes over time under three-point bending

Table 3 Fracture state of three-point bending notched beam on AE hits

Steady state time (time duration), s	Non-steady state time (time duration), s
0-12 (12)	13 (1)
14-29 (16)	30-45 (16)
46-68 (23)	69-70 (2)
71-117 (47)	118-221 (104)
222-600 (379)	601-671 (71)
672-781 (110)	782-848 (67)

Table 4 Analysis results of AE signal parameter and grey-cusp catastrophe model

AE signal parameters	Catastrophe model
Initial compaction stage (53s-87s)	Unstable state (13s, 30s-45s, 69s-70s)
Stable growth stage of micro-cracks (88s-664s)	Unstable state (118s-221s) Stable state (222s-600s)
Crack initiation stage (665s-667s)	Unstable state (601s-671s)
Fracture failure stage (678s-848s)	Stable state (672s-781s) Unstable state (782s-848s)

waves, both ringing count and AE hits were approximately exponential, and the energy releasing rate was large. With load continuing, the fracture zone were further unstable and propagating, eventually leading to the sudden failure.

4.2 Comparison between model analysis results and parameter analysis results

AE signal is a response of crack initiation, propagation and failure in concrete. The catastrophe of specimen fracture will cause the catastrophe of AE signals. Therefore, the catastrophe of signal parameters can be used as the sign of cracking and fracture in the process of concrete failure. It is of great significance to analyze and explore the AE signals from the internal structure of concrete. In order to further investigate the catastrophe characteristics of cracking and fracture process of concrete, a grey-cusp catastrophe model was established based on grey-cusp theory and catastrophe theory. The catastrophe analysis of the cumulative number of AE hits, as shown in Fig. 3(d), was carried out using MATLAB to program calculation and analysis. The specific steps are as follows:

(1) The polynomial fitting, i.e., Eq. (7), was used to fit AGO: $x^{(1)} = \{x^{(1)}(1), x^{(1)}(2), \cdots, x^{(1)}(m)\}$ and the fitting polynomial coefficients $A_1, \ldots, A_5$.

(2) According to the numerical substitution Eq. (11)-(15), the parameters and values of the relationship between mechanical parameters and AE parameters in Eq. (10) were calculated.

(3) The Δ value in Eq. (3) was calculated.

(4) By using the mutation rule and the relationship between bifurcation set equation (Δ and 0), the change of fracture state of three-point bending notched beam was evaluated.

In order to judge the stability of concrete, from the beginning of load to the fracture process, the AE parameters of the experimental process were substituted into the calculation. The calculation results are shown in Table 3.

Fig. 4 Fracture of three point bending beam

In Table 3, it can be seen that under the bending test, the loading process has experienced several stages from stable state to unstable state, and finally to fracture state. The grey-cusp catastrophe model of AE signal was compared with the parameter analysis results as shown in Table 4. The crack evolution process of three-point bending beam can be inferred as following:

(1) Initial compaction stage: The model analysis results show that instability occurred at 15s and 30s-45s. This is due to the contact between the specimen and the loading equipment. Sporadic AE signals began to appear on the contact surface. This phenomenon can also be verified by observation and analysis in the experimental stage. The specimen was in a relatively stable stage. In the compaction stage, only 69s-70s had a sudden-change point, while the parameter analysis only indicated that there were hit counts

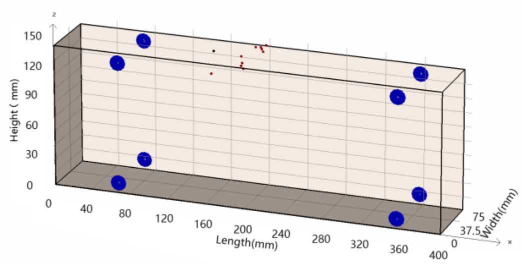

(a) 70s AE crack location

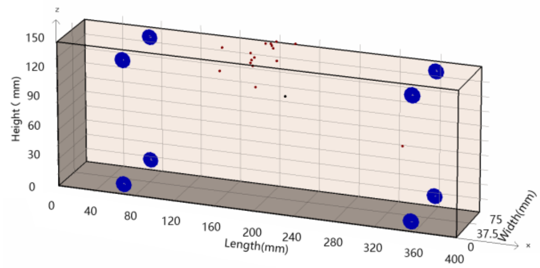

(b) 221s AE crack location

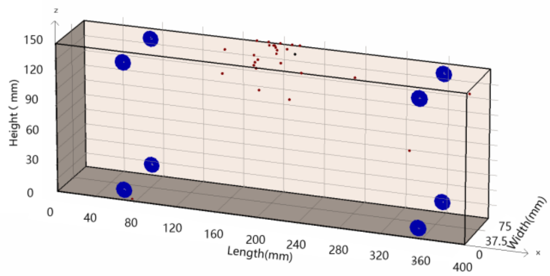

(c) 600s AE crack location

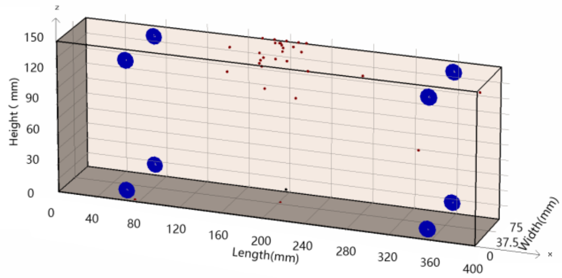

(d) 618s AE crack location

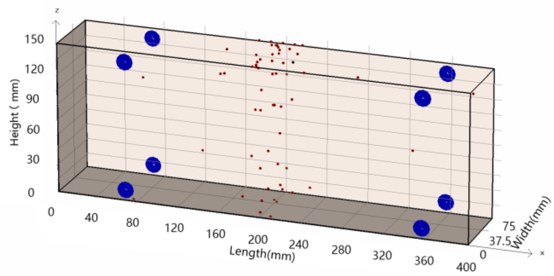

(e) 671s AE crack location

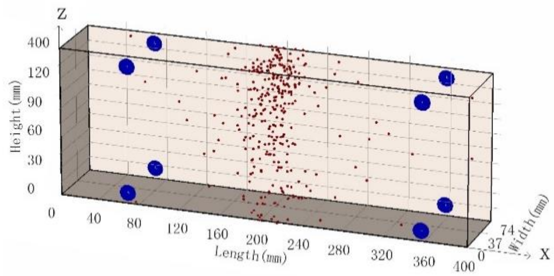

(f) 780s AE crack location

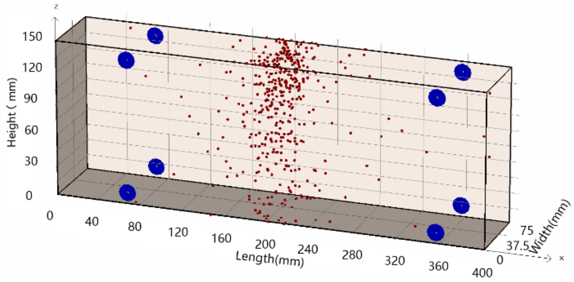

(g) 848s AE crack location

Fig. 5 Crack locations over time during the three-point bending test in 53-87.

(2) Stable growth stage of microcracks: With the continuous loading, the initial cracks in the specimen evolved continuously. In this stage, the occurrence and development of internal cracks in concrete were mainly due to the initial defects, such as microcracks, capillary pores and bleeding pores. The obtained AE signals were mainly produced by these defects, which caused initial fracture under load. As shown in Table 4, within 118s-221s, the system was in an unstable state, but cannot be effectively reflected in the parameter analysis chart (Fig. 3). The less AE signals and the smooth cumulative curve of hit counts revealed that the system was in a stable state from 88s to 664s.

(3) Crack initiation stage: When the internal defects of concrete deformed, cracks expanded to a certain extent, a micro-crack zone in concrete was suddenly penetrated. At this time, macro-crack points appeared in the specimens, which shows that there was an obvious peak value within 665s-667s on the hit counting curve. From the analysis results of the model, it can be seen that the system had a sudden change. This change occurred much earlier than that of the experimental analysis. Comparing with the results of AE test, it can be found that the grey-cusp catastrophe model accurately predicted the crack evolution process of concrete.

(4) Fracture failure stage: The parameter analysis results show that the hit counting curve became steeper, and the concrete was in the fracture failure stage within 678s-848s. The model analysis results can be divided into two stages. With the joint action of crack channel element and barrier element in concrete, the cracks were restrained in the process of propagation. The concrete moved into a new stable state within 672s-781s. In 782s-848s, with load increasing, the microcracks in concrete continued to crack, and then combined to form large cracks. At the same time, new cracks formed, and evolved into one or several micro-crack zones until they developed into macrocracks and fractured. At this point, a new peak appeared in the AE hit counting curve, and the system was in an unstable state until the beam fractured as shown in Fig. 4.

Based on the above comparative analysis, it can be concluded that the grey-cusp catastrophe model not only unified the process of cracking and determine catastrophe state, but also predict crack evolution process in concrete, unstable fracture of concrete, and deduce the degree of fracture. The developed model provided a theoretical foundation for the application of AE in the prediction of concrete fracture.

4.3 Application of the model

Fig. 5 presents crack locations over time in concrete during the three-point bending test. Comparing with Table 3, Fig. 5 perfectly verified the results of catastrophe analysis. As shown from Figs. 5(a)-(g), crack began to appear at the middle of top part on specimen at 70s. The number of cracking points near the top surface was continually increasing until 600s. Then the bottom part of specimen started to exhibit cracking points at 618s. The catastrophe analysis indicates that the specimen had catastrophe at 601s, which was 17 seconds earlier than the AE signal analysis. The specimen kept having more crack points in the tension and compression zones with time. Subsequently, the specimen was in a stable state with a large quantity of crack points appeared. Eventually, the specimen fractured in instability with the most crack points located in concrete. Such crack locations better reflected the crack evolution process of concrete beam under three-point bending test.

5. Conclusions

- The grey-cusp catastrophe model of AE was established based on the cumulative AE parameters which provided an innovative application of AE signals in fracture analysis of concrete. The developed model well described the catastrophe characteristic of concrete.
- AE analysis results were consistent with the experimental results using the grey-cusp catastrophe model and AE parameters better described the crack evolution process of concrete.
- The developed grey-cusp catastrophe model determined the catastrophe state of concrete, predicted the crack evolution process of concrete and provided a theoretical foundation for the application of AE in the prediction of concrete fracture.

Acknowledgements

The study of this paper is financially supported by the National Basic Research Program of China 973 Program (Grant No. 2015CB655103), the Natural Science Foundation of China (Grant Nos. 51678529 and 51978620).

References

Abdelrahman, M.A., ElBatanouny, M.K., Rose, J.R. and Ziehl, P.H. (2019), "Signal processing techniques for filtering acoustic emission data in prestressed concrete", *Res. Nondestr. Eval.*, **30**(3), 127-148. https://doi.org/10.1080/09349847.2018.1426800.

Abouhussien, A.A. and Hassan, A.A.A. (2015), "Evaluation of damage progression in concrete structures due to reinforcing steel corrosion using acoustic emission monitoring", *J. Civil Struct. Hlth Monit.*, **5**(5), 751-765. https://doi.org/10.1007/s13349-015-0144-5.

Asamene, K., Hudson, L. and Sundaresan, M. (2015), "Influence of attenuation on acoustic emission signals in carbon fiber reinforced polymer panels", *Ultrasonics*, **59**, 86-93. https://doi.org/10.1016/j.ultras.2015.01.016.

Barrios, F. and Ziehl, P.H. (2012), "Cyclic load testing for integrity evaluation of prestressed concrete girders", *ACI Struct. J.*, **109**(5), 615-623.

Behnia, A., Chai, H.K. and Shiotani, T. (2014), "Advanced structural health monitoring of concrete structures with the aid of acoustic emission", *Constr. Build. Mater.*, **65**(65), 282-302. https://doi.org/10.1016/j.conbuildmat.2014.04.103.

Carpinteri, A., Lacidogna, G., Niccolini, G. and Puzzi, S. (2008), "Critical defect size distributions in concrete structures detected by the acoustic emission technique", *Meccanica*, **43**(3), 349-363. https://doi.org/10.1007/s11012-007-9101-7.

Choi, C.K. and Cheung, S.H. (1994), "A simplified model for predicting the shear response of reinforced concrete membranes", *Thin Wall. Struct.*, **19**(1), 37-60. https://doi.org/10.1016/0263-8231(94)90004-3.

Choi, C.K. and Cheung, S.H. (1996), "Tension stiffening model for planar reinforced concrete members", *Comput. Struct.*, **59**(1), 179-190. https://doi.org/10.1016/0045-7949(95)00146-8.

Chu, H.Q. and Jiang, L.H. (2009), "Correlation analysis between concrete parameters and electrodeposition effect based on grey theory", *J. Wuhan Univ. Technol.*, **31**(7), 22-26.

Desa, M.S.M., Ibrahim, M.H.W., Shahidan, S., Ghadzali, N.S. and Misri, Z. (2018), "Fundamental and assessment of concrete structure monitoring by using acoustic emission technique testing: A review", *IOP Conf. Ser.: Earth Environ. Sci.*, **140**(1), 012142, April.

Di Benedetti, M., Loreto, G., Matta, F. and Nanni, A. (2013), "Acoustic emission monitoring of reinforced concrete under accelerated corrosion", *J. Mater. Civil Eng.*, **25**(8), 1022-1029. https://doi.org/10.1061/(ASCE)MT.1943-5533.0000647.

Fan, X.Q., Hu, S.W. and Lu, J. (2016), "Damage and fracture processes of concrete using acoustic emission parameters", *Comput. Concrete*, **18**(2), 267-278. https://doi.org/10.12989/cac.2016.18.2.267.

Fu, C., Ye, H., Wang, K., Zhu, K. and He, C. (2019), "Evolution of mechanical properties of steel fiber-reinforced rubberized concrete (FR-RC)", *Compos. Part B: Eng.*, **160**, 158-166. https://doi.org/10.1016/j.compositesb.2018.10.045.

Fu, C.Q., Jin, X.Y., Ye, H.L. and Jin, N.G. (2015), "Theoretical and experimental investigation of loading effects on chloride diffusion in saturated concrete", *J. Adv. Concrete Technol.*, **13**, 30-43. ttps://doi.org/10.3151/jact.13.30.

Huo, L.S., Li, X., Chen, D.D. and Li, H.N. (2017), "Structural health monitoring using piezoceramic transducers as strain gauges and acoustic emission sensors simultaneously", *Comput. Concrete*, **20**(5), 595-603. https://doi.org/10.12989/cac.2017.20.5.595.

Iturrioz, I., Lacidogna, G. and Carpinteri, A. (2013), "Acoustic emission detection in concrete specimens: experimental analysis and simulations by a lattice model", *Int. J. Damage Mech.*, **23**(3), 327-358. https://doi.org/10.1177/1056789513494232.

Jiang, G., Keller, J., Bond, P.L. and Yuan, Z. (2016), "Predicting concrete corrosion of sewers using artificial neural network", *Water Res.*, **92**, 52-60. https://doi.org/10.1016/j.watres.2016.01.029.

Li, B., Cai, L. and Zhu, W. (2017), "Predicting service life of concrete structure exposed to sulfuric acid environment by grey system theory", *Int. J. Civil Eng.*, **12**, 1-11. https://doi.org/10.1007/s40999-017-0251-2.

Li, G.D., Yamaguchi, D. and Nagai, M. (2007), "Prediction of relative dynamic elasticity modulus by extending a grey system theory", *Measur. Sci. Technol.*, **18**(3), 827-834.

Li, X. (2013), "Application of working face rock burst prediction of grey modeling cusp catastrophe analysis based on the acoustic emission", *Appl. Mech. Mater.*, **373-375**, 689-693. https://doi.org/10.4028/www.scientific.net/AMM.373-375.689.

Mainali, G., Dineva, S. and Nordlund. E. (2015), "Experimental study on debonding of shotcrete with acoustic emission during freezing and thawing cycle", *Cold Reg. Sci. Technol.*, **111**, 1-12. https://doi.org/10.1016/j.coldregions.2014.11.014.

Mostafapour, A., Davoodi, S. and Ghareaghaji, M. (2014), "Acoustic emission source location in plates using wavelet analysis and cross time frequency spectrum", *Ultrasonics*, **54**(8), 2055-2062. https://doi.org/10.1016/j.ultras.2014.06.022.

Nair, A. and Cai, C.S. (2010), "Acoustic emission monitoring of bridges: review and case studies", *Eng. Struct.*, **32**(6), 1704-1714. https://doi.org/10.1016/j.engstruct.2010.02.020.

Ohno, K. and Ohtsu, M. (2010), "Crack classification in concrete based on acoustic emission", *Constr. Build. Mater.*, **24**, 2339-2346. https://doi.org/10.1016/j.conbuildmat.2010.05.004.

Pazdera, L., Topolář, L., Daněk, P., Smutny, J. and Mikulášek, K. (2016), "Evaluation of acoustic emission events generated at three point bending of different concrete specimens by spectral analysis", *Solid State Phenomena*, **258**, 485-488. https://doi.org/10.4028/www.scientific.net/SSP.258.485.

Pisani, A.M. (2018), "Behaviour under long-term loading of externally prestressed concrete beams", *Eng. Struct.*, **160**, 24-33. https://doi.org/10.1016/j.engstruct.2018.01.029.

Rodríguez, P. and Celestino, T.B. (2019), "Application of acoustic emission monitoring and signal analysis to the qualitative and quantitative characterization of the fracturing process in rocks", *Eng. Fract. Mech.*, **210**, 54-69. https://doi.org/10.1016/j.engfracmech.2018.06.027.

Sagar, R.V. and Prasad, B.K.R. (2012), "A review of recent developments in parametric based acoustic emission techniques applied to concrete structures", *Nondestr. Test. Eval.*, **27**(1), 47-68. https://doi.org/10.1080/10589759.2011.589029.

Wang, Y., Zhang, Y., Hu, H., Liu, S. and Yuan, L. (2014), "Identification of damage degree of concrete by acoustic emission and artificial neural network", *J. Build. Mater.*, **67**(10), 1497-1497.

Wiedmann, A., Weise, F., Kotan, E., Müller, H.S. and Meng, B. (2017), "Effects of fatigue loading and alkali-silica reaction on the mechanical behavior of pavement concrete", *Struct. Concrete*, **18**(4), 539-549. https://doi.org/10.1002/suco.201600179.

Xie, Z.D., Guan, Y.J., Yu, X.H., Zhu, L.H. and Lin, J. (2018), "Effects of ultrasonic vibration on performance and microstructure of AZ31 magnesium alloy under tensile deformation", *J. Central South Univ.*, **25**(7), 1545-1559.

Xu, J., Barnes, R.W. and Ziehl, P.H. (2013), "Evaluation of prestressed concrete beams based on acoustic emission parameters", *Mater. Eval.*, **71**(2), 176-185.

Yuan, X., Li, B., Cui, G., Zhao, S. and Zhou, M. (2010), "Grey clustering theory to assess the effect of mineral admixtures on the cyclic sulfate resistance of concrete", *J. Wuhan Univ. Technol.*, **25**(2), 316-318.

Yuyama, S., Li, Z.W., Yoshizawa, M., Tomokiyo, T. and Uomoto, T. (2001), "Evaluation of fatigue damage in reinforced concrete slab by acoustic emission", *NDT&E Int.*, **34**(6), 381-387.

Zhai, W., Li, J. and Zhou, Y. (2019), "Application of catastrophe theory to fracability evaluation of deep shale reservoir", *Arab. J. Geosci.*, **12**, 161. https://doi.org/10.1007/s12517-019-4332-1.

Zhou, X., Yang, Y.Y., Li, X.Q. and Zhao, G.Q. (2016), "Acoustic emission characterization of the fracture process in steel fiber reinforced concrete", *Comput. Concrete*, **18**(4), 923-936. https://doi.org/10.12989/cac.2016.18.4.923.

Zohari, M.H., Epaarachchi, J.A. and Lau, K.T. (2013), "Modal acoustic emission investigation for progressive failure monitoring in thin composite plates under tensile test", *Key Eng. Mater.*, **558**, 65-75. https://doi.org/10.4028/www.scientific.net/KEM.558.65

CC